A Numerically Efficient Formulation for Time-Domain Electromagnetic-Semiconductor Cosimulation for Fast-Transient Systems

Quan Chen, Wim Schoenmaker, Guanhua Chen, Lijun Jiang, and Ngai Wong

***Abstract*—We report recent progress in developing a numerically efficient formulation for electromagnetic-technology computer-aided design cosimulation for fast-transient computations. The difficulties underlying the currently existing transient formulation stemming from the vector potential-scalar potential (A-V) framework are analyzed. A time-domain electric field-scalar potential (E-V) framework is then developed via equation and variable transformations. This results in better-conditioned systems that are friendly to iterative solutions at fast switching times. Numerical examples show that the proposed E-V solver renders a useful tool for addressing multidomain simulation.**

***Index Terms*—Cosimulation, E-V framework, electromagnetics, high frequency, TCAD, transient simulation.**

I. Introduction

In RECENT years, there has been a growing demand for combining stand-alone electromagnetic (EM) solvers and technology computer-aided design (TCAD) semiconductor device simulators in mixed-signal, RF, and multidomain simulation. This is because the simplification of semiconductors (to conductors with equivalent conductivity) in linear EM analysis and the neglect of magnetic effects in TCAD simulation have become insufficient to capture the field-carrier interactions that are getting stronger with increasing frequency and decreasing signal level. For instance, the nonlinear interplay between fast-varying EM fields and carrier flows in nonuniformly doped substrates is a subtle but important problem for the allocation of electrostatic discharge structures [1].

The EM-TCAD cosimulation essentially refers to a concurrent solution of the Maxwell's equations that describe the ubiquitous EM dynamics, and the transport equations describing the charge carrier dynamics in semiconductors. A widely tested EM-TCAD framework in the frequency domain was proposed in [2] and [3]. The Maxwell's equations are formulated in terms of scalar potential V and vector potential $\mathbf{A}$ to obtain a straightforward coupling with the drift and diffusion semiconductor model. The A-V formulation has been translated into a series of tools [4], verified against measurements with a number of industrial examples [5], [6], and coupled with the quantum mechanical model to enable multiscale simulation for emerging nanoelectronic devices [7], [8]. Alternative EM-TCAD frameworks have also been reported in [9] and [10].

Whereas the frequency-domain A-V solver has been developed in a rather advanced stage, the transient counterpart so far has been less explored. Unlike the objective of obtaining small-signal response in the frequency domain, the need of transient EM-TCAD simulation comes from the desire to handle large-signal response. A first implementation of time-domain A-V solver was reported recently in [8] and [11]. Due to the extended physical reality and its numerical treatment, five variables are used and solved simultaneously in the formulation. The number of unknowns in each Newton iteration is thus five to six times the number of nodes in the computational grid. The solution process for industrial problems represented in large linearized systems becomes a key concern.

Iterative methods are preferable for solving large sparse linear systems. However, the time-domain A-V formulation in [11] inherits one numerical shortcoming from the frequency-domain counterpart. The iterative solution of the linearized system tends to be increasingly inefficient as the frequency grows beyond 50 GHz. The problem can be traced to the significant off-diagonal blocks in the Jacobian matrix due to the high frequency and metal conductivity. As a remedy, an E-V formulation was developed in the frequency-domain [12], relying on the variable transform (vector potential $\mathbf{A} \rightarrow$ electric field $\mathbf{E}$) and an equation transform for the nodes attached with metals (current continuity $\rightarrow$ gauge condition). The transformations substantially reduce magnitudes of the off-diagonal blocks at high frequencies and a remarkable performance boost of iterative methods has been demonstrated.

In this letter, a time-domain E-V framework is developed for the fast-transient EM-TCAD simulation. Although being based on the similar variable and equation transformations with the frequency-domain E-V method [12], the time-domain E-V solver enables a large-signal coupled simulation at ultra-high-frequencies, which is different from the small-signal analysis in [12]. Furthermore, a new interpretation is provided in this letter to explain the origin of the high-frequency breakdown associated with the A-V solver, and how the E-V solver prevents this numerical difficulty.

II. Time-Domain A-V Formulation

The complete system of equations of time-domain A-V solver is laid out in (1) (with scaling)

$$\begin{cases} \frac{1}{\nu}\nabla\cdot[\varepsilon_r(-\nabla V-\Pi)]-\rho=0,\ \rho=p-n+N_D \\ \frac{1}{\nu}\nabla\cdot\left[\varepsilon_r\left(-\nabla\frac{\partial}{\partial t}V-\frac{\partial}{\partial t}\Pi\right)\right]+\nabla\cdot[\sigma(-\nabla V-\Pi)]+\nabla\cdot\mathbf{J}_{sd}=0 \end{cases} \tag{1a}$$

$$\nabla\cdot\mathbf{J}_n-\frac{\partial}{\partial t}n-R(n,p)=0 \tag{1b}$$

$$\nabla\cdot\mathbf{J}_p+\frac{\partial}{\partial t}p+R(n,p)=0 \tag{1c}$$

$$\frac{\partial}{\partial t}\mathbf{A}-\Pi=0 \tag{1d}$$

$$-K\varepsilon_r\left(-\frac{\partial}{\partial t}\Pi-\nabla\frac{\partial}{\partial t}V\right)-K\nabla\left(\varepsilon_r\frac{\partial}{\partial t}V\right)+ [\nabla\times(\nabla\times\mathbf{A})-\nabla(\nabla\cdot\mathbf{A})]-K\nu\sigma(-\nabla V-\Pi)-K\nu\mathbf{J}_{sd}=0. \tag{1e}$$

Manuscript received July 5, 2012; revised September 26, 2012; accepted November 18, 2012. Date of current version April 17, 2013. This work was supported in part by the Hong Kong University Grant Council under Grant AoE/P-04/08, the Hong Kong General Research Fund Project 718711E, the University Research Committee of the University of Hong Kong, and the European Projects ICESTARS (FP7-ICT-214911) and SQWIRE (FP7-ICT-25711). This paper was recommended by Associate Editor A. Elfadel.

Q. Chen, L. Jiang, and N. Wong are with the Department of Electrical and Electronic Engineering, University of Hong Kong, Pokfulam, Hong Kong (e-mail: quanchen@eee.hku.hk; ljiang@eee.hku.hk; nwong@eee.hku.hk).

W. Schoenmaker is with Magwel NV, Leuven 3000, Belgium (e-mail: wim.schoenmaker@magwel.com).

G. Chen is with the Department of Chemistry, University of Hong Kong, Pokfulam, Hong Kong (e-mail: ghc@everest.hku.hk).

Color versions of one or more of the figures in this paper are available online at http://ieeexplore.ieee.org.

Digital Object Identifier 10.1109/TCAD.2012.2232709

The upper equation in (1a) is the conventional Gauss law, and the lower one represents the current continuity for the nodes attached with metals. Equations (1b) and (1c) are the current continuity equations for electron and holes, where $\mathbf{J}_{sd}$ is the total semiconductor current and R is the net generation/recombination rate. A new variable, called the pseudo-canonical momentum $\Pi=\partial\mathbf{A}/\partial t$, is introduced to avoid the second-order time derivative acting on the vector potential [11]. Equation (1e) represents a modified Maxwell–Ampere (MA) equation that includes the subtraction of the divergence of Lorentz gauge condition

$$\nabla\cdot\mathbf{A}+K\varepsilon_r\frac{\partial V}{\partial t}=0 \tag{2}$$

to eliminate the singularity of the curl–curl operator [12] by conversion to a Laplacian form. K and ν are two dimensionless scaling parameters that will be discussed later.

The system after spatial discretization can be assembled in a matrix format as shown in (3). V_1 and V_2 are partitioned according to the different governing equations in (1a). Similarly, Π is divided into Π_1 and Π_2 for the links attached without and with metallic volumes, respectively. I denotes the identity matrix with the appropriate dimension.

Equation (3) can be further condensed to a nonlinear differential equation

$$C\dot{x}=-Gx-F(x)-b \tag{4}$$

where C and G collect the linear dynamics in the system, F collects the nonlinear dynamics (generally the nonlinear semiconductor currents), and b is the source term.

In a temporal regime, (4) is generally discretized by a backward differential formula (BDF). For simplicity, here we employ the first-order BDF, i.e., the BE discretization. Newton's method is employed to handle the nonlinear algebraic system generated by BE. The linearized equation to be solved at the $k+1$th Newton iteration of the $n+1$ time step is therefore

$$\left(J_F+\frac{C}{h}+G\right)\Delta x_{n+1}^{k+1}= -\left(F(x_{n+1}^{k})+\left(\frac{C}{h}+G\right)x_{n+1}^{k}-\frac{C}{h}x_n+b_{n+1}\right) \tag{5}$$

where $J_F=\frac{\partial F}{\partial x}\big|_{x_{n+1}^k}$ is the partial derivatives of nonlinear semiconductor currents and h is the time step size.

III. Analysis of Fast-Transient Breakdown

A slightly modified version of the generalized de Mari scaling in [3] is applied to (1) to improve the numerical range of the physical quantities that may differ by orders of magnitude. In particular, four independent scaling parameters, λ for length, τ for time, n_i for doping and carrier concentrations and V_T for scalar potentials, are pre-determined, from which the remaining scaling parameters are derived from their physical relation. The length scaling λ is usually chosen to be the natural length scale of the problem under consideration to render the matrix entries generated by differential operators of magnitude $O(1)$. The time scaling τ is selected according to the natural time scale of the problem to make $h/\tau\sim O(1)$. The dimensionless parameters K and ν are defined by $K=\mu_0\varepsilon_0(\lambda/\tau)^2$ and $\nu=qn_i\lambda^2/(\varepsilon_0V_t)$, respectively, with ε_0 and μ_0 being the vacuum permittivity and permeability.

Performance of the iterative solution of (5) depends on the eigenvalue distribution of the Jacobian matrix $J=\left(\frac{\partial F}{\partial x}\big|_{x_{n+1}^k}+\frac{C}{h}+G\right)$. To further facilitate the analysis, we focus on the contribution of the linear components (e.g., back-end structures) to the Jacobian matrix by forming an M matrix as in (6), which includes only the blocks related to $(V,\mathbf{A},\Pi)$. The displacement currents on metal nodes/links can be omitted compared with the conduction currents ($\sigma\gg\varepsilon_r/\nu$). The existence of semiconductor would generally not affect results of the following analysis, and will be discussed at the end of Section IV:

$$M=\begin{bmatrix}\begin{bmatrix}-\frac{1}{\nu}\nabla\cdot(\varepsilon_r\nabla)\\-\nabla\cdot(\sigma\nabla)\end{bmatrix} & 0 & \begin{bmatrix}-\frac{1}{\nu}\nabla\cdot\varepsilon_r\\-\nabla\cdot\sigma\end{bmatrix}\\ 0 & I & -I\\ \begin{bmatrix}K(\varepsilon_r\nabla-\nabla\varepsilon_r)\\K\nu\sigma\nabla\end{bmatrix}\begin{bmatrix}\nabla^2\\\nabla^2\end{bmatrix} & \begin{bmatrix}K\varepsilon_r\\K\nu\sigma\end{bmatrix}\end{bmatrix}. \tag{6}$$

Here the conductivity $\sigma=\sigma_0/s_\sigma$ has been scaled by $s_\sigma=\varepsilon_0\nu/\tau$, where σ_0 is the real metal conductivity.

Similar to the frequency-domain counterpart [12], the time-domain formula (6) has off-diagonal blocks depending on the the large value of metal conductivity, which is unfavorable for the generalized minimal residual (GMRES) convergence. This numerical difficulty can be alleviated by further row (block) scaling to make the matrix have approximately an equal row (block) norm. The M matrix after row balancing becomes

$$M=\begin{bmatrix}\begin{bmatrix}-\nabla\cdot(\varepsilon_r\nabla)\\-\nabla\cdot(\nabla)\end{bmatrix} & 0 & \begin{bmatrix}-\nabla\cdot\varepsilon_r\\-\nabla\cdot\end{bmatrix}\\ 0 & I & -I\\ \begin{bmatrix}K(\varepsilon_r\nabla-\nabla\varepsilon_r)\\\nabla\end{bmatrix}\begin{bmatrix}\nabla^2\\\nabla^2/(K\nu\sigma)\end{bmatrix} & \begin{bmatrix}K\varepsilon_r\\1\end{bmatrix}\end{bmatrix}. \tag{7}$$

It is evident from (7) that M has generally balanced blocks except the $\nabla^2/(K\nu\sigma)$ one, which decreases linearly with the reciprocal of τ, or the frequency of interest, since

$$K\nu\sigma=\mu_0\sigma_0\frac{\lambda^2}{\tau}\propto\frac{1}{\tau}. \tag{8}$$

While the $\nabla^2/(K\nu\sigma)$ term becomes smaller at fast transients, the last and second rows in (7) become increasingly close to each other (differing by only a divergence operator), rendering the resultant Jacobian an ill-conditioning matrix. The matrix will even become singular when the term $\nabla^2/(K\sigma)$ vanishes. This intuitively explains the difficulty in an iterative solution the A-V solver encounters when simulating systems with rapid-varying dynamics.

An in-depth analysis can be conducted by looking at the original unscaled physical system. As pointed out in [12], the combination of the current continuity (9a) and the original MA equation (9b) would lead to a redundant system. To eliminate the redundancy, the divergence of the gauge condition is subtracted from the original MA equation, resulting in (9b) [or the scaled version in (1e)]

$$\nabla\cdot\left(\varepsilon\frac{\partial\mathbf{E}}{\partial t}+\sigma\mathbf{E}+\mathbf{J}_{sd}\right)=0 \tag{9a}$$

$$[\nabla\times(\nabla\times\mathbf{A})-\nabla(\nabla\cdot\mathbf{A})]-\mu\left(\sigma\mathbf{E}+\varepsilon\frac{\partial\mathbf{E}}{\partial t}+\mathbf{J}_{sd}\right)=0. \tag{9b}$$

$$\begin{bmatrix} \begin{bmatrix} 0 \\ -\frac{1}{\nu}\nabla\cdot(\varepsilon_r\nabla) \end{bmatrix} & \begin{bmatrix} 0 \\ -\frac{1}{\nu}\nabla\cdot\varepsilon_r \end{bmatrix} & & & & \\ & I & & & & \\ & & I & & & \\ & & & I & & \\ \begin{bmatrix} K(\varepsilon_r\nabla-\nabla\varepsilon_r) \\ K(\varepsilon_r\nabla-\nabla\varepsilon_r) \end{bmatrix} & & \begin{bmatrix} K\varepsilon_r \\ K\varepsilon_r \end{bmatrix} & & & \end{bmatrix} \begin{bmatrix} \begin{bmatrix} \dot{V}_1 \\ \dot{V}_2 \end{bmatrix} \\ \dot{n} \\ \dot{p} \\ \dot{A} \\ \begin{bmatrix} \dot{\Pi}_1 \\ \dot{\Pi}_2 \end{bmatrix} \end{bmatrix} = - \begin{bmatrix} \begin{bmatrix} -\frac{1}{\nu}\nabla\cdot(\varepsilon_r\nabla) \\ -\nabla\cdot(\sigma\nabla) \end{bmatrix} & \begin{bmatrix} I_n \\ 0 \end{bmatrix} & \begin{bmatrix} -I_p \\ 0 \end{bmatrix} & & \begin{bmatrix} -\frac{1}{\nu}\nabla\cdot\varepsilon_r \\ -\nabla\cdot\sigma \end{bmatrix} \\ & 0 & & & \\ & & 0 & & \\ & & & 0 & -I \\ \begin{bmatrix} 0 \\ K\nu\sigma\nabla \end{bmatrix} & & & \begin{bmatrix} \nabla^2 \\ \nabla^2 \end{bmatrix} & \begin{bmatrix} 0 \\ K\nu\sigma \end{bmatrix} \end{bmatrix} \begin{bmatrix} \begin{bmatrix} V_1 \\ V_2 \end{bmatrix} \\ n \\ p \\ A \\ \begin{bmatrix} \Pi_1 \\ \Pi_2 \end{bmatrix} \end{bmatrix} - \begin{bmatrix} \begin{bmatrix} 0 \\ \nabla\cdot\bar{J}_{sd} \end{bmatrix} \\ -\nabla\cdot\bar{J}_n + R \\ \nabla\cdot\bar{J}_p + R \\ 0 \\ \begin{bmatrix} -K\nu\bar{J}_{sd} \\ -K\nu\bar{J}_{sd} \end{bmatrix} \end{bmatrix} - \begin{bmatrix} \begin{bmatrix} -N_D \\ 0 \end{bmatrix} \\ 0 \\ 0 \\ 0 \\ \begin{bmatrix} 0 \\ 0 \end{bmatrix} \end{bmatrix} \tag{3}$$

The efficiency of this remedy depends on the magnitude contrast between the first and the second term of (9b). Since the surface integral $\iint_{\Delta S}[\nabla\times(\nabla\times)-\nabla(\nabla\cdot)]ds$ gives an $O(1)$ magnitude in the spatial discretization, the magnitude of the first term is $O(\mathbf{A})$. The magnitude of the second term, if on a metallic link, would be dominated by (the surface integral of) the conduction current, which is on the order of $O(\lambda^2\mu_0\sigma_0\mathbf{E})$ (λ is selected to be the natural length scale of the mesh). For typical materials $\mu_0\sigma_0\sim O(1)$, and for fast transients $O(\mathbf{E})\sim O(\frac{\partial\mathbf{A}}{\partial t})=O(\frac{\mathbf{A}}{\tau})$, where τ represents the natural time scale of the problem. Then, the magnitude of the second term will have a dependence on the ratio λ^2/τ. When this ratio is large, e.g., at high frequencies or with fast transients, the Laplacian term in (9b) will be overwhelmed by the conduction current, leaving the equation to represent nothing but a zero total current on the link, and cause difficulty when solved together with the node-wise current continuity equation (9a). Since such magnitude imbalance occurs in the same equation on the same unknown ($\mathbf{A}$), any row or column scaling cannot prevent (9b) from getting close to the current continuity as τ decreases. From this perspective, the numerical difficulty of the A-V formulation is generally scaling independent.

A question that follows immediately is, when the conduction current term in (1e) will dominate the equation, or when $K\nu\sigma$ will become large. One can see from (8) that the definition of fast transient depends on the ratio of λ^2/τ. When $\tau\approx\lambda^2$ the fast-transient breakdown starts to occur with the A-V formulation. For μm-scale structures where $\lambda\approx 10^{-6}$, breakdown starts to occur for $\tau\approx 10^{-12}$, which roughly corresponds to 50 GHz ($\tau\sim 1/20$ of period), consistent with finding in the frequency domain in [12]. For nanoscale problems with $\lambda\approx 10^{-9}$, τ can be up to 10^{-18}, meaning that the A-V solver will generally not encounter severe problems until 10^{17}Hz. In addition, if no metals are included in the simulation, the redundancy problem can largely be avoided.

IV. Time-Domain E-V Formulation

We have revealed that the numerical problem of the A-V solver for fast-transient systems results from the concurrent solution of the current continuity and the modified MA equation in the metallic region. A natural remedy will hence be replacing the current continuity in the metals [the lower one in (1a)] by the gauge condition (2) as in [12]. It is a valid equation transformation provided that it is only applied on the nodes attached with metallic volumes, while keeping the original Gauss's law for the remaining nodes. This way, redundancy is avoided even when the modified MA equation collapses to the current continuity equation for fast transients.

Meanwhile, the comparable diagonal and off-diagonal blocks in (7) are not desirable for fast convergence of iterative methods, which is attributed to the A-V potential formulation of Maxwell's equations where the electric field $\mathbf{E}$ is separated into V and Π components but still used as an entity in the expression of displacement current. Therefore, a variable transformation $\mathbf{E}=-\nabla V-\Pi$ is employed to minimize the cross-coupling between V and Π in the relevant equations. The complete E-V equation system is laid out in (10)

$$\begin{cases} \frac{1}{\nu}\nabla\cdot(\varepsilon_r\mathbf{E})-\rho=0,\ \rho=p-n+N_D \\ K\varepsilon_r\frac{\partial}{\partial t}V+\nabla\cdot\mathbf{A}=0 \end{cases} \tag{10a}$$

$$\nabla\cdot\mathbf{J}_n-\frac{\partial}{\partial t}n-R(n,p)=0 \tag{10b}$$

$$\nabla\cdot\mathbf{J}_p+\frac{\partial}{\partial t}p+R(n,p)=0 \tag{10c}$$

$$\nabla V+\frac{\partial}{\partial t}\mathbf{A}+\mathbf{E}=0 \tag{10d}$$

$$-K\varepsilon_r\frac{\partial}{\partial t}\mathbf{E}+K\nabla\left(-\varepsilon\frac{\partial}{\partial t}V\right)+[\nabla\times(\nabla\times\mathbf{A})-\nabla(\nabla\cdot\mathbf{A})] -K\nu\sigma\mathbf{E}-K\nu\mathbf{J}_{sd}=0. \tag{10e}$$

Analogous to the analysis of A-V solver, the M matrix in the E-V solver is constructed for $(V,\mathbf{A},\mathbf{E})$ as

$$M=\begin{bmatrix} \begin{bmatrix} 0 \\ K\varepsilon \end{bmatrix} & \begin{bmatrix} 0 \\ \nabla\cdot \end{bmatrix} & \begin{bmatrix} \frac{1}{\nu}\nabla\cdot\varepsilon_r \\ 0 \end{bmatrix} \\ \nabla & I & I \\ \begin{bmatrix} K\nabla\varepsilon_r \\ K\nabla\varepsilon_r \end{bmatrix} & \begin{bmatrix} -\nabla^2 \\ -\nabla^2 \end{bmatrix} & \begin{bmatrix} K\varepsilon_r \\ K\nu\sigma \end{bmatrix} \end{bmatrix}. \tag{11}$$

One additional merit of the E-V formulation lies in the improved diagonal dominance of the last row of (11). The large metal conductivity only appears at diagonals, which in the meanwhile increases linearly with respect to the frequency as $K\sigma\sim 1/\tau$. The drawback of the E-V solver is that the diagonal term $K\varepsilon_r$ in the gauge condition is small when frequency is low, rendering high off-diagonal dominance that affects the performance of iterative methods. Nevertheless, this term increases quadratically with the reciprocal of the time step, $K\sim 1/\tau^2$. Therefore, the E-V solver will have better performance in high-frequency simulations, similar to its counterpart in the frequency domain.

The role that doped semiconductor plays depends largely on the doping density. For typical doping densities used in semiconductor devices, the equivalent conductivities of semiconductor are approximately $10\sim 10^3 S/m$, four orders smaller than that of metal ($\sim 10^7 S/m$). This means that the time step needs to be four orders smaller as well to cause the same problem as in the metal case. Therefore, the inclusion of a doped semiconductor would generally not hamper the efficiency of the E-V solver. On the other hand, if degenerately doped semiconductors with comparable conductivity with metals (e.g., polysilicon gate electrodes) are included, the same numerical difficulty may still occur for the E-V solver, because

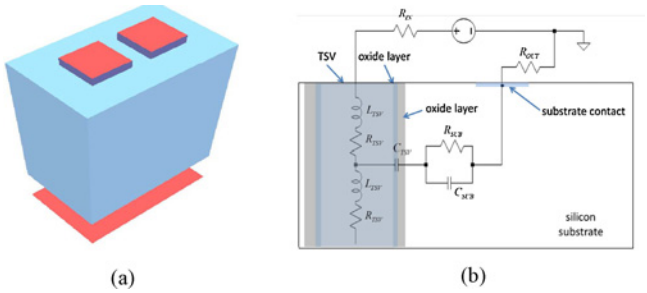

Fig. 1. TSV structure. (a) 3-D view. (b) Equivalent circuit model. One copper TSV with $4 \times 4\,\mu\text{m}^2$ cross-section is surrounded by an oxide layer of $0.1\,\mu$m thickness, and embedded in a $16 \times 10\,\mu\text{m}^2$ silicon substrate. The TSV and the substrate contact are separated by $5\,\mu$m. The substrate has a thickness of $20\,\mu$m, and a uniform p-type doping of $2 \times 10^{15}\,\text{cm}^{-1}$.

the current continuity and MA equations are solved again simultaneously in these metal-like regions. In this case, it might be reasonable to treat such types of semiconductors as metals in matrix assembling, provided that the charge carrier distribution inside these semiconductors is not of research interest.

V. Numerical Results

The time-domain A-V and E-V solvers were both implemented in MATLAB and tested with three structures. The first one is a through-silicon via (TSV) structure motivated by a recent work [13] to model the nonlinear coupling between a TSV and an adjacent substrate contact through a doped substrate. The geometric details and the equivalent circuit model are shown in Fig. 1. The other two structures are a substrate noise isolation structure and an 8-shaped inductor in voltage controlled oscillator (VCO), whose details can be found in [11] and [12], respectively. GMRES was used in the iterative solutions, along with the threshold-based incomplete LU (ILUT) preconditioner and the column approximate minimum degree (COLAMD) permutation to reduce fill-ins in the preconditioner. This combination represents the state of the art in iterative solutions of large sparse linear systems. All tests were conducted on a 3.2 GHz 32 Gb-RAM computer.

First, the validity of the E-V formulation is verified by comparing with the A-V solver in Fig. 2 using the TSV structure. A 25 GHz sinusoidal wave with the amplitude of 2 V (at 0 bias) is applied to the TSV and the induced voltage is measured at the substrate contact, which represents the noise coupling through the substrate. A constant step size $h = 10^{-12}$s and the direct linear solver (backslash in MATLAB) were used. It is seen that the A-V and E-V curves overlap on the top of each other, which is expected since no approximation is introduced with the variable and equation transformations.

The TSV example can be also used to demonstrate the usefulness of EM-TCAD cosimulation. It was reported in [13] that the bias voltage can influence the electric characteristics of TSV via modulating the width of depletion layer in substrate. The increase of depletion layer width at depletion mode will decrease the total TSV capacitance [C_{TSV} in Fig. 1(b)], which in turn reduces the strength of substrate coupling. Fig. 3 shows the induced voltage with the same sinusoidal input as above but with different DC biases. When a bias of $DC = -4V$ is applied, the TSV will stay in accumulation mode during the whole simulation, rendering a roughly constant C_{TSV} equal to the oxide capacitance and an approximately linear output response. At a DC=0V bias, however, the input voltage changes the TSV capacitance over time during the simulation and induces nonlinear distortion in output voltage (the falling edge). For further comparisons, we also simulate the structure using an equivalent conductivity model ($\sigma_{eq} = 24S/m$) for the silicon substrate. Again two different biases were applied. The two simulated waveforms are in phase with each other and the EM-TCAD results with $-4V$ bias, indicating that the equivalent conductivity model cannot capture the voltage-dependence of TSV capacitance on applied voltage. This effects will be more significant at high frequencies when more power leakage occurs via the capacitive substrate path.

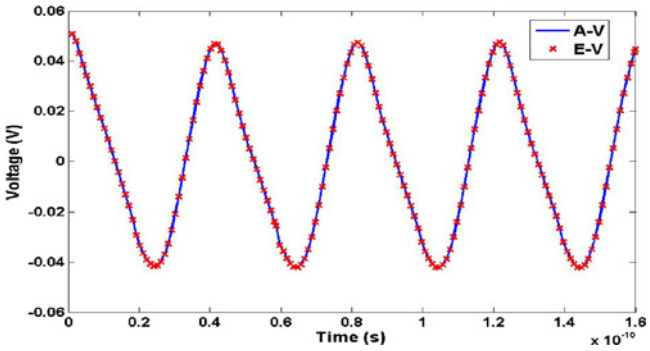

Fig. 2. Induced voltage in the TSV structure calculated by A-V and E-V solvers.

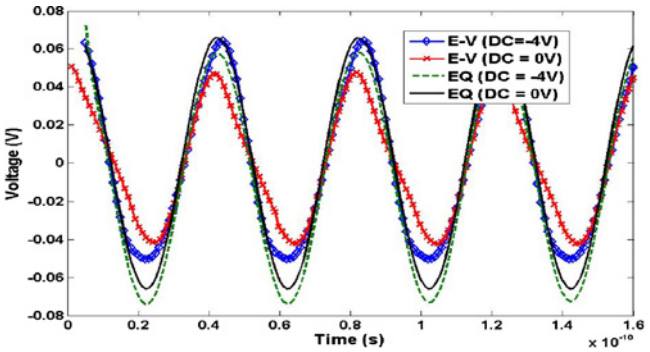

Fig. 3. Induced voltage in the TSV structure for different bias voltages and with equivalent conductivity model.

The GMRES performance of the A-V and the E-V solvers with different step sizes are compared in Table I. The corresponding frequency range is roughly 100 MHz∼100 THz. The same COLAMD+ILUT(10^{-3})+GMRES combo is applied in all cases. t_{pre} denotes the time for constructing the ILUT preconditioner. t_{GMRES} and N_{it} are the total time of GMRES and the number of iterations required to achieve the tolerance of 10^{-8}, respectively. Symbol $-$ indicates failure in computing preconditioner or getting convergence within 300 iterations

As demonstrated in Table I, the numerical systems arising from the A-V formulation are favorable for iterative solutions for slow-transient systems. As the necessary time step decreases, the convergence rate of GMRES continuously slows down and failures occur for extremely small step sizes. The E-V solver behaves in an opposite manner. The GMRES

TABLE I
PERFORMANCE OF ITERATIVE SOLUTION IN A-V AND E-V SOLVERS

Case	Matrix Size	h	A-V			E-V		
			t_{pre}	t_{GMRES}	N_{it}	t_{pre}	t_{GMRES}	N_{it}
TSV	18 599	1e-09	2.11	0.58	15	14.14	28.61	164
		1e-11	2.59	0.66	16	11.09	2.52	19
		1e-13	9.63	18.58	176	10.64	2.34	15
		1e-15	–	–	–	4.77	3.05	9
SUB	41 368	1e-09	5.91	9.75	86	–	–	–
		1e-11	7.41	12.91	96	15.89	4.65	19
		1e-13	18.72	84.35	298	16.88	5.01	20
		1e-15	–	–	–	5.87	1.29	11
VCO	149 898	1e-09	59.61	1.59	3	–	–	–
		1e-11	649.65	583.87	195	834.23	356.77	87
		1e-13	–	–	–	461.23	281.39	56
		1e-15	–	–	–	180.94	236.49	52

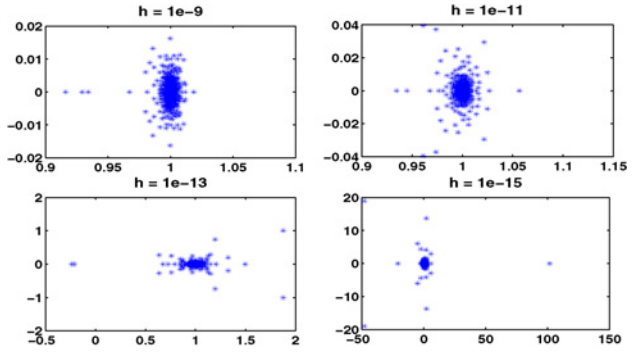

Fig. 4. Eigenvalue distribution of A-V solver with different step sizes (preconditioned Jacobian matrix $U^{-1}L^{-1}M$ of the TSV case).

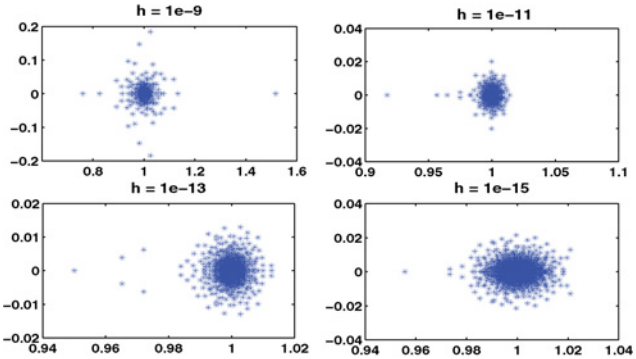

Fig. 5. Eigenvalue distribution of E-V solver with different step sizes (preconditioned Jacobian matrix $U^{-1}L^{-1}M$ of the TSV case).

convergence is slow at lower frequencies. For systems with fast-varying dynamics, however, the E-V solver outperforms the A-V solver substantially, suggesting that the E-V solver will be a valuable tool for EM-TCAD coanalysis in RF or an even higher frequency range. The convenient switch between A-V and E-V solvers [12] also enables a wide-band simulation across the preferred regions of both solvers.

Spectral analysis is further conducted to explain the frequency-dependent behaviors of A-V and E-V solvers in Figs. 4 and 5. The eigenvalues of the preconditioned Jacobian are shown for different step sizes. ILUT (10^{-5}) is used to ensure that preconditioners can be constructed for all step sizes. The eigenvalues in the A-V solver cluster tightly around the unity at slow transients, but spread away at fast transients. The smaller is the step size, the more outlying eigenvalues appear, indicating a poor GMRES convergence rate. The spectrum of E-V solver follows a reversed trend. The eigenvalues are much more clustered for small time steps than for large time steps, which is consistent with the observations in Table I.

VI. CONCLUSION

We revealed that the time-domain EM-TCAD cosimulation based upon the existing A-V formula will encounter numerical difficulty when simulating metallic structures at fast switching times. An E-V formulation was developed by equation and variable transformations to improve the conditioning of the numerical systems and thus to enhance the efficiency of iterative solvers. It was demonstrated that the E-V solver leads to a significant speedup for fast-transient systems, and would, therefore, be a useful tool for multidomain simulation involving fast transients.

REFERENCES

[1] P. Galy, J. Jimenez, W. Schoenmaker, P. Meuris, and O. Dupuis, "ESD RF protections in advanced CMOS technologies and its parasitic capacitance evaluation," in *Proc. IEEE Int. Conf. IC Des. Technol.*, May 2011, pp. 1–4.

[2] P. Meuris, W. Schoenmaker, and W. Magnus, "Strategy for electromagnetic interconnect modeling," *IEEE Trans. Comput.-Aided Des.*, vol. 20, no. 6, pp. 753–762, Jun. 2001.

[3] W. Schoenmaker and P. Meuris, "Electromagnetic interconnects and passives modeling: Software implementation issues," *IEEE Trans. Comput.-Aided Des.*, vol. 21, no. 5, pp. 534–543, May 2002.

[4] Magwel [Online]. Available: http://www.magwel.com/

[5] *CODESTAR—Compact Modeling of On-Chip Passive Structures at High Frequencies* [Online]. Available: http://www.magwel.com/codestar/

[6] *ICESTARS—Integrated Circuit/EM Simulation and Design Technologies for Advanced Radio Systems-on-Chip* [Online]. Available: http://www.icestars.eu

[7] C. Yam, L. Meng, G. Chen, Q. Chen, and N. Wong, "Multiscale quantum mechanics/electromagnetics simulation for electronic devices," *Phys. Chem. Chem. Phys.*, vol. 13, no. 32, pp. 14 365–14 369, Aug. 2011.

[8] L. Meng, C. Yam, S. Koo, Q. Chen, N. Wong, and G. Chen, "Dynamic multiscale quantum mechanics/electromagnetics simulation method," *J. Chem. Theory Comput.*, vol. 8, no. 4, pp. 1190–1199, Feb. 2012.

[9] G. F. Wang, R. W. Dutton, and C. S. Rafferty, "Device-level simulation of wave propagation along metal-insulator-semiconductor interconnects," *IEEE Trans. Microw. Theory Tech.*, vol. 50, no. 4, pp. 1127–1136, Apr. 2002.

[10] F. Bertazzi, F. Cappelluti, S. D. Guerrieri, F. Bonani, and G. Ghione, "Self-consistent coupled carrier transport full-wave EM analysis of semiconductor traveling-wave devices," *IEEE Trans. Microw. Theory Tech.*, vol. 54, no. 4, pp. 1611–1617, Apr. 2006.

[11] W. Schoenmaker, M. Matthes, B. D. Smedt, S. Baumanns, C. Tischendorf, and R. Janssen, "Large signal simulation of integrated inductors on semi-conducting substrates," in *Proc. Des. Autom. Test Eur.*, Mar. 2012, pp. 1221–1226.

[12] Q. Chen, W. Schoenmaker, P. Meuris, and N. Wong, "An effective formulation of coupled electromagnetic-TCAD simulation for extremely high frequency onwards," *IEEE Trans. Comput.-Aided Des.*, vol. 30, no. 6, pp. 866–876, Jun. 2011.

[13] J. Cho, J. Kim, J. S. Pak, J. Lee, H. Lee, K. Park, and J. Kim, "Nonlinear effects of TSV and harmonic generation," in *Proc. IEEE Electron. Compon. Technol. Conf.*, Jun. 2012, pp. 834–838.